Title
Co-Solvency in Liquid Exfoliation of Layered Materials

Author
Zheng, Chu Ran

Publication Date
2012

Peer reviewed|Thesis/dissertation

UNIVERSITY OF CALIFORNIA

Los Angeles

Co-Solvency in Liquid Exfoliation of Layered Materials

A thesis submitted in partial satisfaction

of the requirements for the degree Master of Science

in Chemistry

by

Chu Ran Zheng

2012

ABSTRACT OF THE THESIS

Co-Solvency in Liquid Exfoliation of Layered Materials

by

Chu Ran Zheng

Master of Science in Chemistry

University of California, Los Angeles, 2012

Professor Xiangfeng Duan, Chair

The extraordinary physical properties of layered inorganic materials have become a tremendous breakthrough in prominent electronic related applications. Due to the growing number of application in these materials, simple methods that produce high quality in larger quantities are highly desired. This thesis describes a novel method in exfoliating the layered inorganic materials with versatile solvents via co-solvency approach. This research demonstrates how mixtures of different common solvents with water could significantly improve the exfoliation of layered materials compared to its pure solution. The most efficient solvent mixtures for exfoliating the layered materials are those with the co-solvent in larger molecular size and surface energy close to that of the nanosheets. For all the solvent mixtures examined in this study, solvent mixtures that best exfoliate the materials tends to have co-solvent/water mixing ratio that gives surface tension of 22-28mN/m in the case of exfoliating graphene and 22-

30mN/m for MoS_2. The solvent mixtures are ranked in the following trend that based on their exfoliation ability: *tert*-Butanol-Water > Isopropanol-Water > Ethanol-Water > Acetonitrile-Water > Methanol-Water. Finally, the exfoliated materials are fabricated into thin film via interfacial solution process.

The thesis of Chu Ran Zheng is approved.

Richard B. Kaner

Yu Huang

Xiangfeng Duan Committee Chair

University of California, Los Angeles

2012

Table of Contents

List of Figures

Acknowledgments

This thesis represents not only the end of my academic endeavor but also a major milestone of a prolonged distressed and dedication journey yet amazing chapter in my life.

I would like to thank my God Almighty, Jesus Christ, who never leaves me during my struggle and distraught time. I am grateful for His countless blessing to give me strength and encouragement to achieve this astonishing opportunity to have a higher level of education.

Through the past one year, it has been neither easy nor straightforward. Yet, I have met some astounding scientists and extraordinary scholars who have helped me along this very exciting experience in my academic venture.

First, I want to say my sincere gratitude to **Professor Xiangfeng Duan** as my wonderful research advisor. It was all started in Spring 2011 during my undergraduate year. It was my very first time to have a chance to talk and interact with him closely in Chem 185 class with him as the primary instructor. Prof. Duan took a major part in helping me to shape my decision in pursuing this master degree. Prof. Duan has always been my inspiration and encouragement for the past year. His conscientious and positive work ethics have always been my role model and constructive motivation. I would not be where I am today without his never-ending support and guidance in doing my research in Co-Solvency in Liquid Exfoliation of Layered Materials. His practical approach and drive in Chemistry have taught me immeasurable experience to value science and its breakthrough potential in an immense and enriched perspective.

Next, I want to thank **Udayabagya Halim** as my supportive graduate mentor. Udayabagya is a remarkable mentor who I love to work with. His insightful advice and energetic conduct have encouraged me to always give my 110% towards my work in the lab. I am more than glad to have him as my graduate mentor. I am more than comfortable to work together and discuss anything that I am not sure with him. Udayabagya has been working with me for countless hours for the past year, trying to figure out every obstacle that we found in this research thesis. I am grateful that I have learned a lot from him, not only in terms of scientific approach but also how I deal with every problem that I may encounter in the next chapter in my life.

I would also thank my parents for their unconditional love and support, not only for the past year in my graduate year but also throughout every struggle that I have been through in my life. I have been living far away from them for the past three years ever since I got admitted into UCLA. Still, their reassurance and faith on me have never failed to brace me during my hardest times.

And the last but not the least, I want to thank my wonderful boyfriend, Christopher Djunaedi. I want to thank him for his never-ending mental support and commitment for the past 4 years, and especially the past year.

It has been an extraordinary year for me, both academically and in my personal life. It was not an easy ride but I have learned priceless and countless lesson, not only limited as in a science

subject, but which makes me who I am today and in the future. Thank you so much for all of you. God bless you all.

1

Introduction

1.1 Motivation

In 2004, Geim and Novosolv [1] established a new stage for materials science by discovering the first atomically thin two-dimensional (2D) material, graphene, with mechanical cleavage. It is found that graphene owns unique mechanical and electronic properties such as quantum electronic transport [2-3], a tunable band gap [4], extremely high mobility [5] and high elasticity [6] and electromechanical modulation [7]. Those distinct characteristics have evolved from narrowed applications to a new era with promising applications in the next-generation electronic devices.

As of today, many believe that graphene is the major key to transform innovative electronic devices [8-11] (i.e.: transparent wearable electronics, displays, and photovoltaic devices). Inspired by the discovery of graphene properties, 2D materials with similar properties with graphene have analogously attracted tremendous attention as novel material properties are found when structure dimensionality approaches to atomic scale [12]. These 2D materials include boron nitride and transition metal dichalcogenides. Recently, monolayer molybdenum disulfide and tungsten disulfide have exhibited direct band gap property that opens new possibility for atomic thin electronic [13,14]. As a result, fabrication methods that produce these materials with high yields and large quantities in large-area are favorably demanded. Up to date, synthesis of freestanding 2D materials is mainly divided into three routes: vapor deposition, lithium

intercalation, and liquid-phase process. Lithium intercalation route [18,28] has by far ranked with the least favored as numerous studies have shown that chemical structure of the material is changed after the intercalation process, in which lowers the material's performances. Vapor deposition is ranked with the most preferred method in terms of preserving pristine material properties. Various studies have successfully demonstrated that molybdenum disulfide [16], boron nitride [17] and graphene [15] films could grow by chemical vapor deposition (CVD) on substrates. However, as it has been mentioned before that a simple method that can produce in large quantities is highly desired for the development of these materials. Thus, top-down approach with liquid-phase process has shown as an alternative to vapor deposition due to its superiority in manufacturing cost, scale-up production, and preserve pristine chemical properties [18].

1.2 Objective

Researchers from all over the world have been studying the efficiency of producing sheets of inorganic compounds with atomic thickness in liquid-phase exfoliation since the early 1960s [19]. Recently, Coleman *et al*. [20] have successfully dispersed a rich collection of layered inorganic materials in various common liquid solvents such as N-Methyl-2-pyrrolidone (NMP) and Dimethylsulphoxide (DMSO) by ultrasonication. However, due to the high surface energy of these layered inorganic materials, the best solvents tend to be those with high boiling points. As a result, post-processing method has become challenging, as these nonvolatile solvents are hard to remove. Currently, Zhou *et al*. [21] have demonstrated that highly stable inorganic graphene analogues can be obtained in low boiling co-solvency mixtures (ethanol and water) when non-solvent pair is mixed in appropriate composition. This solvent mixing strategy that employs

volatile solvents has struck the exfoliation limit as compared to when the solvents are used individually.

However, the choice of solvent pair is challenging since they need to have the right physical properties in order for them to work. Therefore, the objective of this research is to develop a systematic study of the alcohol/water co-solvency system and exert a relationship between surface tension and optimal exfoliation, as well as exfoliation rate with co-solvent molecular weight.

1.3 Approach

In this alcohol/water co-solvency system study, Graphite and MoS_2 were selected as the raw materials, where MoS_2 was selected to represent the transition metal dichalcogenides group layered materials. Methanol, Ethanol, Isopropanol, and *tert*-Butanol were chosen to be the co-solvent since they are the common used solvents and all of them shared similar properties. By replacing the –H with the $–CH_3$ group on the alcohol molecule, the solubility effect due to small changes in its chemical properties was studied. Then, alcohol was replaced by acetonitrile to demonstrate the solubility effect due to the polar group change of the hydroxyl (–OH) group with the nitrile (–C≡N) group. Lastly, exfoliation rate on various solvent compositions was examined by sonication time study.

2

Background of Study and Literature Review

2.1 General

The background theories, which are relevant to this thesis, will be presented in this chapter. First, the structure and chemical properties of inorganic layered materials such as graphene and transition metal dichalcogenides will be described. Next, the criteria for solvent selection and the role of each parameter will be addressed through a brief description of some of the experimental examples and models that have been developed. Lastly, the previous solvent-mixed studies based on co-solvency system will be explained and summarized.

2.2 Inorganic Layered Materials

Inorganic layered materials are bulk materials with structure consisting of their 2D counterparts that are vertically stacked through van der Waals bonding forces. Graphene and transition metal dichalcogenides are one of the typical examples and are described below.

Graphite [22] is a 3D solid consisting of stacked graphene layers where each layer is formed with carbon atoms arranged in honeycomb structure, as shown in Figure 1. Each carbon bonds are sp^2 hybridized where the in-plane σ C-C bond is one of the strongest bonds in materials. The out-of-plane π bond is responsible for the delocalization of the π orbital electrons in which accounts for carbon electrical conductivity and provides the weak interactions between the layers or substrate.

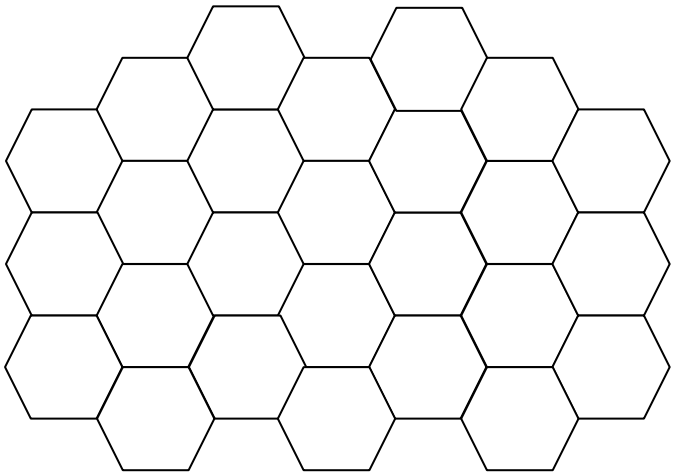

Figure 1. Structure of a single 2D graphene sheet.

Transition metal dichalcogenides [23] are compounds with stoichiometry chemical formula of MX_2 where M represents the transition metal element with formal oxidation state of 4+ and X represents the chalcogenide ion of X^{2-}. The main structure types are those such as MoS_2, WS_2, $MoSe_2$, $NbSe_2$, and $NiTe_2$. By varying the metal and the chalcogenide, material's electrical properties can be ranging from semiconducting to superconducting [24]. The crystal structure of MX_2 sheet is arranged in the form of X-M-X sandwich stack (Figure 2) with each stacking plane arranged in the hexagonal form. The basal plane of the MX_2 sheet is very stable as each chalcogenide atom is fully coordinated with the metal atoms through covalent interaction.

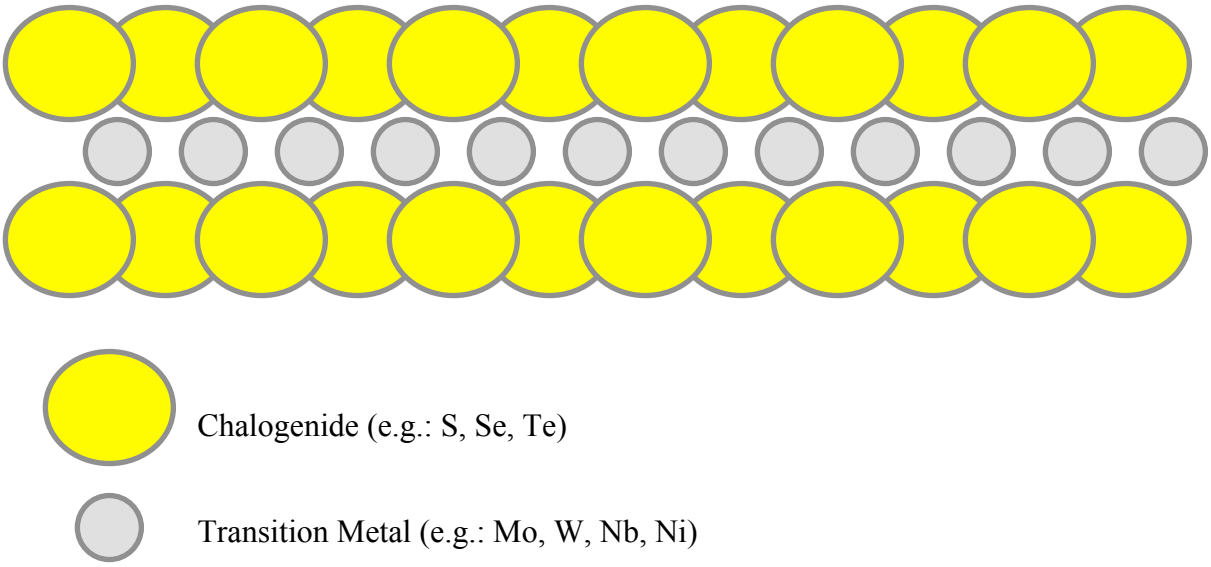

Figure 2. Crystal structure of a single MX_2 sheet.

2.3 Criteria for Solvent Selection

Recently, Coleman *et al.* [20, 25] have shown sonication of inorganic layered compounds in solvents that can produce few-layer nanosheets with lateral dimensions of a few hundred nanometers effectively. However, dispersed concentration was found varied significantly from solvent to solvent. Due to the inconsistent dispersion results and dissolution behavior in only some of the solvents, a correlation between the chemical structure of the exfoliated nanosheet and their dispersability in solvents are established, in which is developed based on two empirical theories: surface energy and Hansen solubility parameters. Now, these two parameters have become the major guidelines in designing or selecting solvents for the non-covalent solution-phase process of inorganic layered materials [26]. The summary on these two parameters will be presented below.

2.3.1 Surface Tension / Surface Energy

Basic Principle of Surface Tension & Surface Energy in Solid and Liquid [50]

Surface in solids and liquids represents the termination of the phase where the atoms or molecules are not bonded in all directions and only surrounded by other atoms or molecules on only one side. The existent of the uneven bonding arise an imbalance of forces at these surface atoms or molecules, and surface energy is the term used to describe this imbalance force where it is the excess energy per unit area that corresponds to the surface with the unsatisfied bonds. The units of surface energy are J/m^2. The tendency to minimize the total surface energy by minimizing the surface is described by surface tension and given in units of N/m. The relation between the two can be described by the following equation where work done per unit increase of area is:

$$\frac{\mathrm{d}(\mathrm{A}\gamma)}{\mathrm{dA}} = \gamma + \frac{\partial\gamma}{\partial\mathrm{A}} \quad (\mathrm{Eq.}\ 1)$$

A is the surface area and γ is surface energy. As shown from the equation, surface tension and surface energy are equal for isotropic materials (i.e.: liquids), but different for anisotropic solids. In thermodynamic, the most stable state is the one with the least free energy. For isotropic liquid, its structure tends to stay in a form with minimum area/unit volume (i.e.: sphere) due to its molecular mobility. This means the term $\partial\gamma / \partial A$ is zero in the case for liquid; thus surface tension and surface energy are numerically the same even when area is changed. For anisotropic solids, surface energy of a crystal depends on its crystallographic orientation. Moreover, surface energy changes when surface atoms are compressed or pulled apart, leading to a $\partial\gamma / \partial A$ value. Therefore, surface tension does not equal to surface energy for solids.

The Role of Surface Energy in Solvent Selection

Surface energy has widely been used as one of the solubility parameters in selecting solvents for carbon nanotubes, graphene and graphene analogues [20, 21, 25, 26]. Numerous studies have suggested that the best solvents in dispersing these layered materials are those tend to have surface energy close to that of the dispersing solids. This phenomenon can be explained by using Gibbs free energy equation:

$$\Delta G_{mix} = \Delta H_{mix} - T\Delta S_{mix} \quad \text{(Eq. 2)}$$

ΔG_{mix} is the Gibbs free energy, ΔH_{mix} is the enthalpy of mixing, T is the temperature, and ΔS_{mix} is the entropy of mixing. For an ideal mixture, enthalpy of mixing approaches to zero and gives a highly favored negative free energy value that indicates the system occurs spontaneously. In 2008, Bergin *et al*. [27] applied this thermodynamic modeling by explaining the exfoliation of carbon nanotubes in solvents. Later, Cunningham *et al*. [26] adopted Bergin *et al*.'s approach and developed a similar model in study of the balance of Van der Waals interaction under solvent-nanosheet conditions. Based on their modeling, the enthalpy of mixing can be approximated by the following equation:

$$\frac{\Delta H_{mix}}{V} \approx \frac{2}{T_{NS}}\left(\sqrt{\gamma_{NS}} - \sqrt{\gamma_{sol}}\right)^2 \phi \quad \text{(Eq. 3)}$$

V is the volume of the mixture, T_{NS} is the nanosheet thickness, γ_{NS} and γ_{sol} are the nanosheet and solvent surface energy, respectively, ϕ is the dispersed nanosheet volume fraction. As shown,

this equation predicts that the optimal dispersing condition occurs when solvent surface energy is very close to the nanosheet.

2.3.2 Hansen Solubility Parameters (HSP)

Hansen Solubility Parameters have existed since 1967 and it provides a useful means to predict molecular affinities, solubility and solubility-related phenomena [29]. The idea is based on the concept of "like dissolve like" as each molecule is assigned with three parameters built from theses following attractions forces: dispersion forces (δ_D), permanent dipole-permanent dipole forces (δ_P), and hydrogen bonding (δ_H). The fundamental principle of HSP concludes that if a solute's solubility parameters are not too different from the one of the selected solvent; subsequently, they will have high affinity and dissolve. Likewise, each parameter can be treated as a three-dimensional (3D) coordinates in a 3D graph. A material's solubility can thus be characterized by the distance between its location to the point representing the solvent. This relation can be described by using the following equation:

$$R_a = \sqrt{4(\delta_{D,sol} - \delta_{D,NS})^2 + (\delta_{P,sol} - \delta_{P,NS})^2 + (\delta_{H,sol} - \delta_{H,NS})^2} \quad \text{(Eq. 4)}$$

R_a is the interaction radius; $\delta_{D,sol}$, $\delta_{P,sol}$, and $\delta_{H,sol}$ are the dispersion, polar, and H-bonding for solvent, respectively; $\delta_{D,NS}$, $\delta_{P,NS}$, and $\delta_{H,NS}$ are the dispersion, polar, and H-bonding for nanosheet, respectively. Thus, mixture with higher solubility arises from those with smaller interaction radius value. For the case of multi-components solvent, HSP theory can also be applied to the solvent mixture as each of the HSP parameters can be calculated from the following equation:

$$\delta_{\text{blend}} = \sum \phi_{\text{comp,n}} \delta_{\text{comp,n}} \quad \text{(Eq. 5)}$$

$\phi_{comp,n}$ and $\delta_{comp,n}$ are the volume fraction and the intrinsic HSP parameter value of the specific component in the solvent mixture, respectively.

2.4 Co-solvency System

Co-solvency phenomenon was first discovered during the research of a cellulose nitrate solution system in 1920 [30]. It was interestingly found that a pair of non-solvents could essentially act as a good solvent and dissolve a polymer when mixed in some specific compositions [31]. In contrast to co-solvency, a different phenomenon was observed in a pair of good solvents mixture where it showed poorest solvent power in a polymer and termed Co-non-solvency [32]. A typical example of the co-solvency phenomenon can be seen from the dissolution process of a thermoplastic polymer, poly(methyl methacrylate) (PMMA), in non-solvent pairs such as carbon tetrachloride with alcohols (Methanol, Ethanol, Propanol, and Butanol) [34] or water with alcohol [33]. In the co-solvency system of water/2propanol/PMMA, Cowie *et al.* [33] proposed that a ternary system in the combination of water/PMMA and 2propanol/PMMA contacts were produced in the mixing state, in which these contacts are of a different nature and sufficient to cause the polymer to dissolve. These contacts are based on like-contacting-like manner, such that there are possible specific site interactions between PMMA (carbonyl group) and water via hydrogen bonding. Moreover, it is also believed that the mixture of both ethanol and water would give a specific polarity that are suitable to dissolve the polymer chains while pure water would be too polar and alcohol is too non-polar to dissolve the polymer.

Though, solubility studies of solvent mixtures based on co-solvency or co-non-solvency approach has been well studied in the field of polymer and pharmaceuticals science; yet, similar study approach has rarely applied to inorganic materials due to the lack of structural analogues to thermoplastic polymers where the systems which only exhibit Van der Waals or dispersive-type interactions are required. Now, layered inorganic materials are an excellent medium to be used in studying the effect of co-solvency due to the weak Van der Waals interaction between the layers. The very first solvents-mixed strategy for dispersing inorganic materials was reported by Zhou *et al.* [21] in 2011. They examined various composition of water and ethanol mixtures along with employing the solvent selections criteria proposed by Coleman *et al.* to achieve a highly stable suspension under ambient conditions.

3

Experimental Method

3.1 Materials and Method

3.1.1 Materials

Graphite and MoS_2 were purchased from Sigma Aldrich. Both materials were obtained in powder with ≥ 95% pure. In all cases the powder were used as purchased.

3.1.2 Instruments

Ultrasonication-assisted dispersion process was carried out with VWR Ultrasonic Cleaner (B2500A-DTH, 210W). Centrifugation was carried out with Eppendorf MiniSpin® plus. UV-Vis absorption and transmittance spectroscopy were performed by DU-800 spectrophotometer.

3.2 General Procedure

3.2.1 Sample Preparations

In all cases, 10mg of powder sample was added to a 10mL glass vial. Then 5mL of water/alcohol mixtures with mass percent of 0 to 100% was added as dispersion solvent.

3.2.2 Sonication and Centrifugation Process

All samples were batch sonicated for 3 hours with each sample placed in different position in the sonic bath every ½ hour cycle to give uniform power distribution. Resulting dispersion was centrifuged at 14,500rpm for 5 minutes. The supernatant was decanted by pipette followed by another centrifugation at 14,500rpm for 15 minutes.

3.2.3 Thin Films Fabrication

Concentrated exfoliated material was mixed with Butanol in 1:1 ratio and added drop-wisely onto the DI water surface. After sufficient amount of materials were added, freestanding film was formed on the surface of the DI water after as all the butanol evaporated. Then, freestanding film was scooped by silylated substrate. Finally, the film was annealed at 200°C under vacuum environment for 10 hours to remove excessive solvents. Scheme of the thin film process is shown below.

(A) Solution of decant containing exfoliated graphene in 30 mass% of Isopropanol was mixed with 1:1 ratio of Butanol

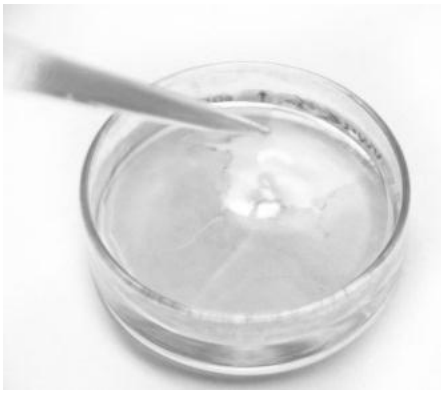

(B) Ready-to-fabricate-graphene mixture was added onto the DI water surface drop wisely and freestanding graphene formed as Butanol evaporated.

(C) Freestanding film on DI water surface was scooped by substrate.

Figure 3. Schematic illustration of graphene films fabrication process.

4

Results and Discussion

4.1 Dispersion Characterization

Photographs of the typical supernatant of graphite and MoS_2 nanomaterials dispersed in various compositions of isopropanol/water mixtures are shown in Figure 4 and Figure 5, respectively. As shown in both images, color intensities of the suspensions varied significantly with different isopropanol/water mixtures compositions, in which indicated that different concentration of dispersed graphite and MoS_2 nanomaterials were obtained. For example, at 30 mass % of isopropanol, dark gray dispersion of graphite and dark yellowish-green dispersion of MoS_2 were obtained, while light gray and light yellow dispersion were observed for graphite and MoS_2 in pure isopropanol, respectively. Such results suggested that co-solvency system could successfully enhance the dispersion concentration with the appropriate non-solvents ratio. Moreover, these suspensions are highly stable under ambient condition over periods of weeks as no sedimentation was observed.

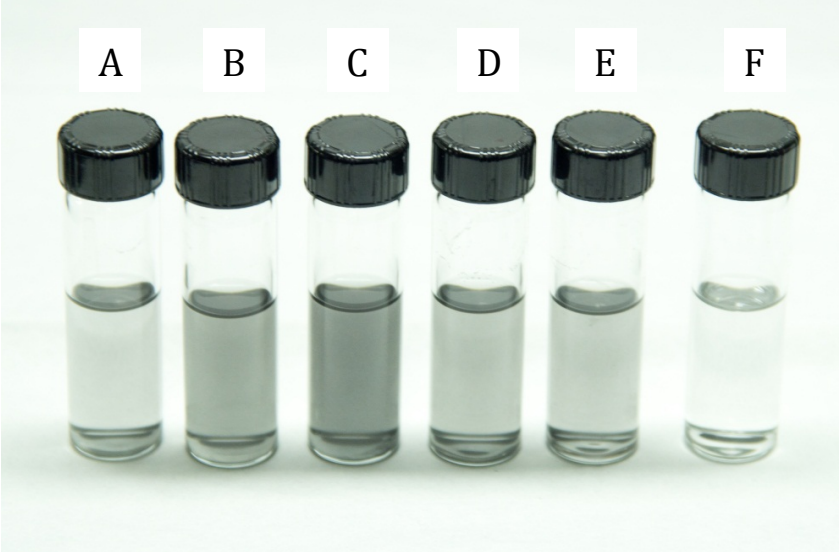

Figure 4. (A) - (F) Exfoliated Graphite in 10 mass%, 30 mass%, 40 mass%, 50 mass%, 80 mass%, and 100 mass% Isopropanol, respectively.

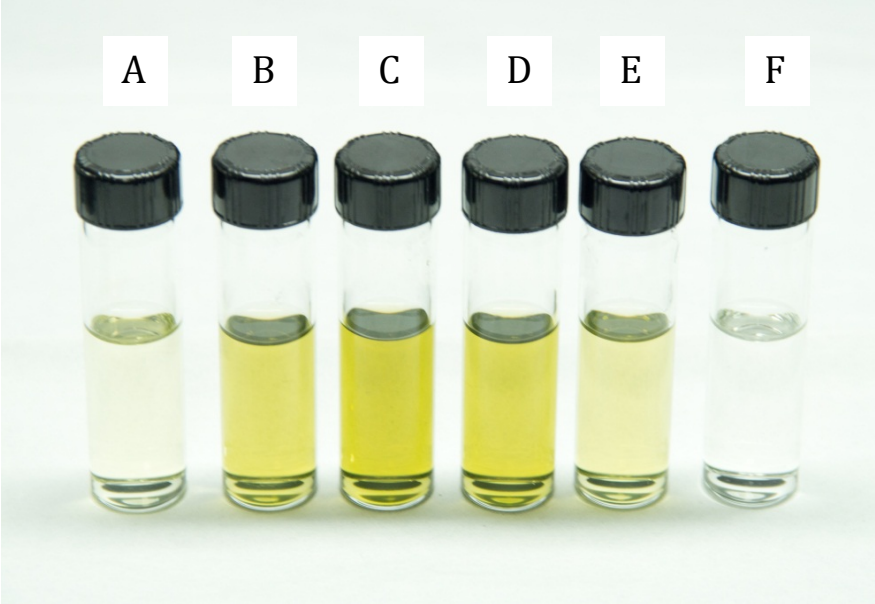

Figure 5. (A) - (F) Exfoliated MoS_2 in 10 mass%, 30 mass%, 40 mass%, 50 mass%, 60 mass%, and 100 mass% Isopropanol, respectively.

4.2 Optical Characterization

Optical absorption spectroscopy was used to characterize the concentration of the materials retained in the dispersions. We used the Lambert-Beer law to relate the absorbance and the dispersed concentration by the following equation:

$$A = \varepsilon Cl \quad (Eq. 6)$$

Where A is the absorbance, ε is the absorption coefficient, C is the concentration of the compound in solution and l is the path length of the sample. As shown in Equation 6, absorbance is proportional to the concentration of the dispersed materials.

Typical absorbance spectra of graphite and MoS_2 suspension in 30 mass% of *tert*-Butanol are shown in Figure 6. Both spectra showed feature that was expected for both materials [35,36] and graphene oxide absorption band (peak at ~231nm)[35] was not observed in Figure 6(A), which indicated the absence of unflavored side reaction during the process.

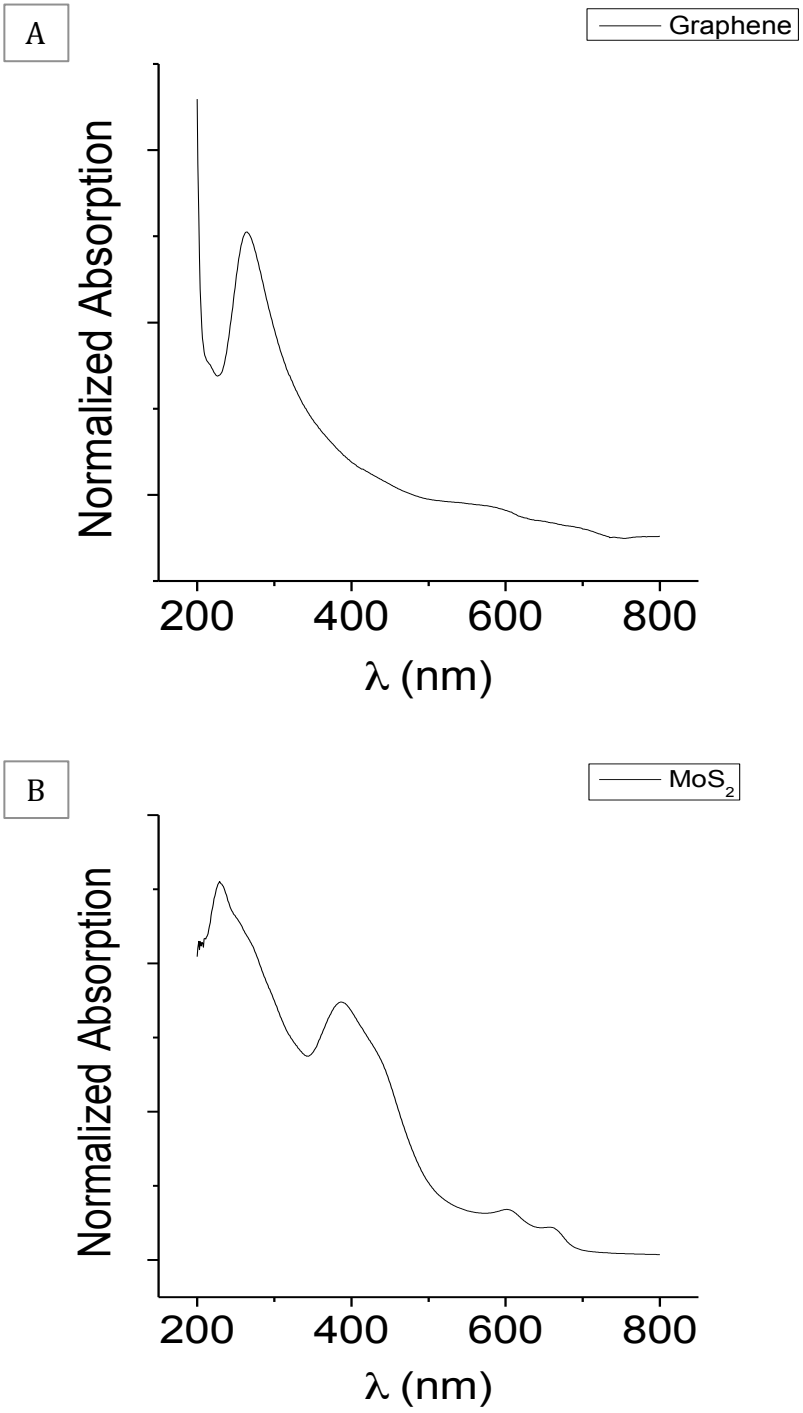

Figure 6. Absorbance spectra for exfoliated (A) Graphite and (B) MoS_2 in 30 mass% *tert*-Butanol.

The absorbance of graphite and MoS_2 suspensions in different alcohol/water mixtures with different composition are shown in Figure 7. The mass percent of the co-solvent was converted to its corresponding surface tension value and plotted against the measured absorbance. A trend was observed in both graphite and MoS_2 materials where larger solvents performed the best in exfoliating the materials. Figure 7(A)–(B) clearly show that Methanol has very little exfoliation while *tert*-Butanol almost exfoliate 20x more than Methanol. In addition, as the co-solvent concentration increased, an increase of the concentration of the graphite and MoS_2 dispersions were observed followed by a decrease in concentration when co-solvent to water ratio approached to 100%. Where it also shows a good agreement with the photographs shown in Figure 4 and Figure 5.

In Figure 7(C) and 7(D), all four mixtures that have alcohols as the co-solvent show that their exfoliation of graphene and MoS_2 could reach the maximum at solvent surface tension close to around 22-28mN/m and 22-30mN/m, respectively. Such results can be understood by the surface energy theory that successful solvents are those with surface energy close to the surface energy of the nanosheet. Surface energy for graphite has been reported to have a wide range of values from as low as 55mJ/m^2 by contact angle measures [37] up to ~70mJ/m^2 by solubility measurements [25]. Similarly, surface energy for MoS_2 has also been reported with value from as low as 49mJ/m^2 by using exponential-sixth and Lennard- Jones potential calculation [38] up to ~75mJ/m^2 by solubility measurement [26]. In addition to that, surface free energy per surface is half of the generally reported value, because it only takes into account the contribution of one surface instead of two. Therefore, by combining all these references, our experimental results are

relatively consistent with our prediction that dispersed concentration is maximized when overall enthalpy of the system is minimized as described in Equation 4.

In the case of MoS_2 in different composition of Ethanol-Water mixtures, similar absorbance trend was obtained as compared to the one reported by Zhou *et al.* [21] in which they showed that the highest dispersion concentration for MoS_2 was obtained at 45vol% of Ethanol-Water mixture, where surface tension is 30.16mN/m. Therefore, our results clearly show a good agreement with theirs. Also, based on their interaction radius (R_a) calculation, 45vol% of Ethanol-Water mixture has the smallest value and in consistent with HSP theory.

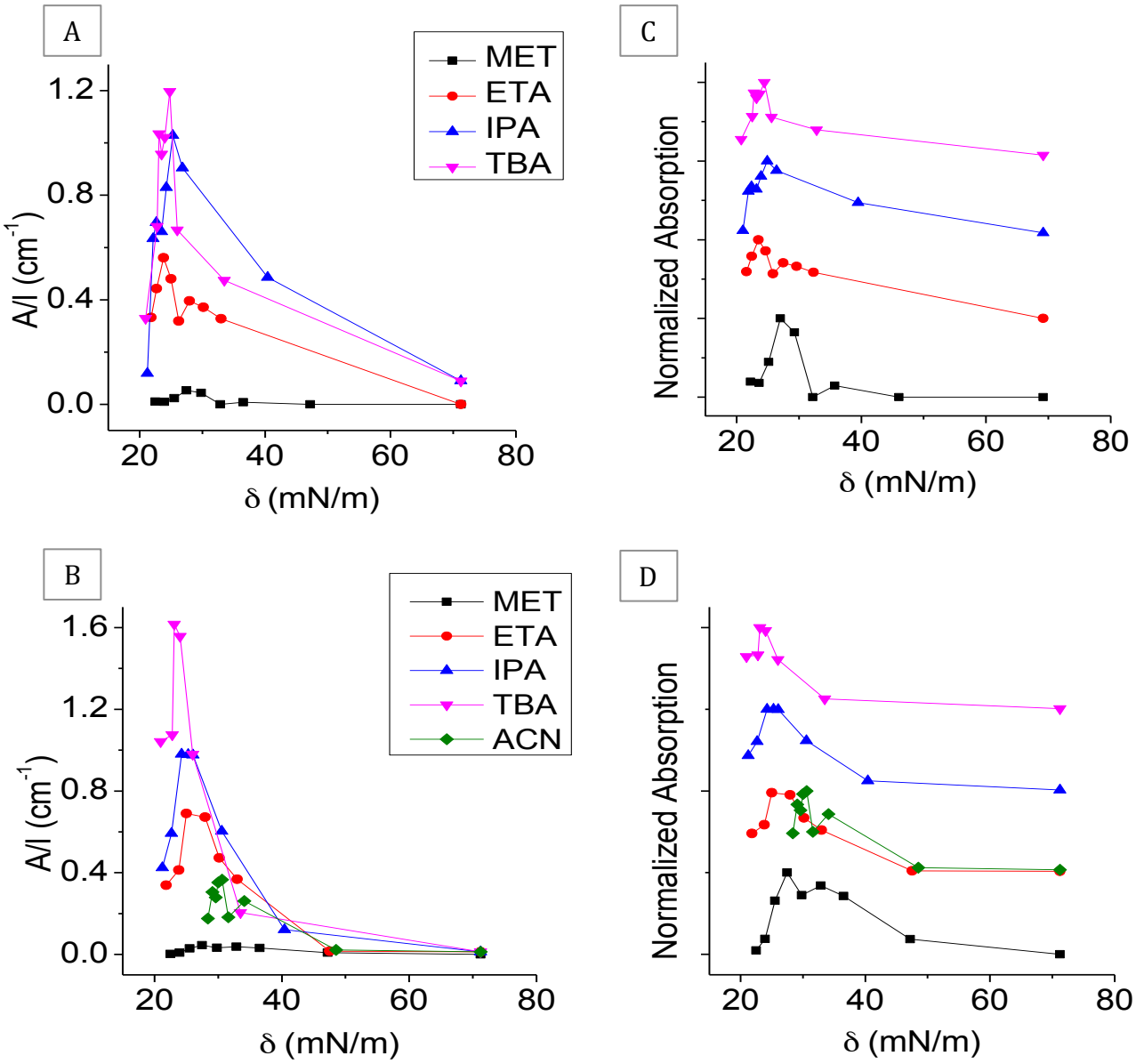

Figure 7. Absorption spectra for exfoliated (A) graphite at 260nm and (B) MoS_2 at 385nm in various solvent mixtures are plotted as a function of surface tension that corresponds to its respective co-solvent mass percent. (C) and (D) are the normalized absorption spectra of graphite (4A) and MoS_2 (4B), respectively; for peak position determination. (MET = Methanol, ETA = Ethanol, IPA = Isopropanol, TBA = *tert*-Butanol, ACN = Acetonitrile).

In addition, Acetonitrile was replaced as the co-solvent to test the polar group change of the hydroxyl (–OH) group with the nitrile (-C≡N) group for the case of MoS_2. The results are presented in Figure 7(B) and 7(D). Instead of peaking around at 22-28mN/m like the other alcohols co-solvent, the maximum exfoliation peak shifted toward 29-31mN/m instead. It is important to note that the surface tension of pure Acetonitrile was reported to have a value of 28.4mN/m. Due to this limitation; it would not reach the approximate peak for MoS_2 that is centered on ~25mN/m. Although the value is slightly higher than the one observed when alcohols were used as the co-solvent, the optimum exfoliation condition still falls in the range where its surface energy value are close to the one belongs to MoS_2.

4.2.1 Co-solvent Analysis

Results shown above indicate that larger co-solvent molecules tend to perform better at dispersing the materials. Such interesting trend can be explained by the steric repulsive interaction occurred between the confined solvent molecules and the sheets. Study done by Shih *et al.* [39] on graphite exfoliation with various organic solvent suggested that solvent molecules provides steric (Leonard-Jones Potential) repulsion that prevents the layers of sheets to reach a specific inter-sheet separation distance such that the attraction force in between the sheets are strong enough to overcome the energy barrier and recombined by desorbing the solvent molecules. Although the study was only examined on a single solvent system, we suggest that similar argument could be made to the solvent-mixing system, such that steric repulsion that responsible for preventing recombination between layers is contributed to the size of the solvent molecules.

Maximum absorbance versus co-solvent molecular weight in dispersing graphene and MoS_2 are shown in Figure 8. Data points were extracted from the absorbance spectra. As clearly shown in Figure 8, the data resemble a straight line in which depicts a linear relation between the co-solvent's molecular weight and its dispersive ability. It is shown that *tert*-Butanol-Water mixtures provide the largest overall concentration at equilibrium while Methanol-Water mixtures show practically no exfoliation. Evidently, *tert*-Butanol-Water mixture provides superior stability for exfoliation condition due to its large molecular size as compared to the rest. Thus, sufficient separation distance is provided in between the sheets with dispersing the materials in a stable manner.

All the solvent mixtures tested were reported with a low viscosity value [51]. We believe that viscosity effect towards centrifugation process is limited. Even though viscosity and density of the solvent mixtures might affect the results, the significant difference of the exfoliation of material in *tert*-Butanol-Water, Isopropal-Water and Ethanol-Water only varies in the factor of 2. Such observation would not yield in over 20 times difference between the exfoliation of Methanol-Water and other solvents based on its sedimentation coefficient. Thus, viscosity was not taken into account in this study.

Same reasoning can be applied to results observed for Acetonitrile where its exfoliation maxima lay below Ethanol-Water mixture but above Methanol-Water mixtures. It is mainly contributed to its molecular size where it's molecular weight falls between Ethanol and Methanol as shown in Figure 8(B).

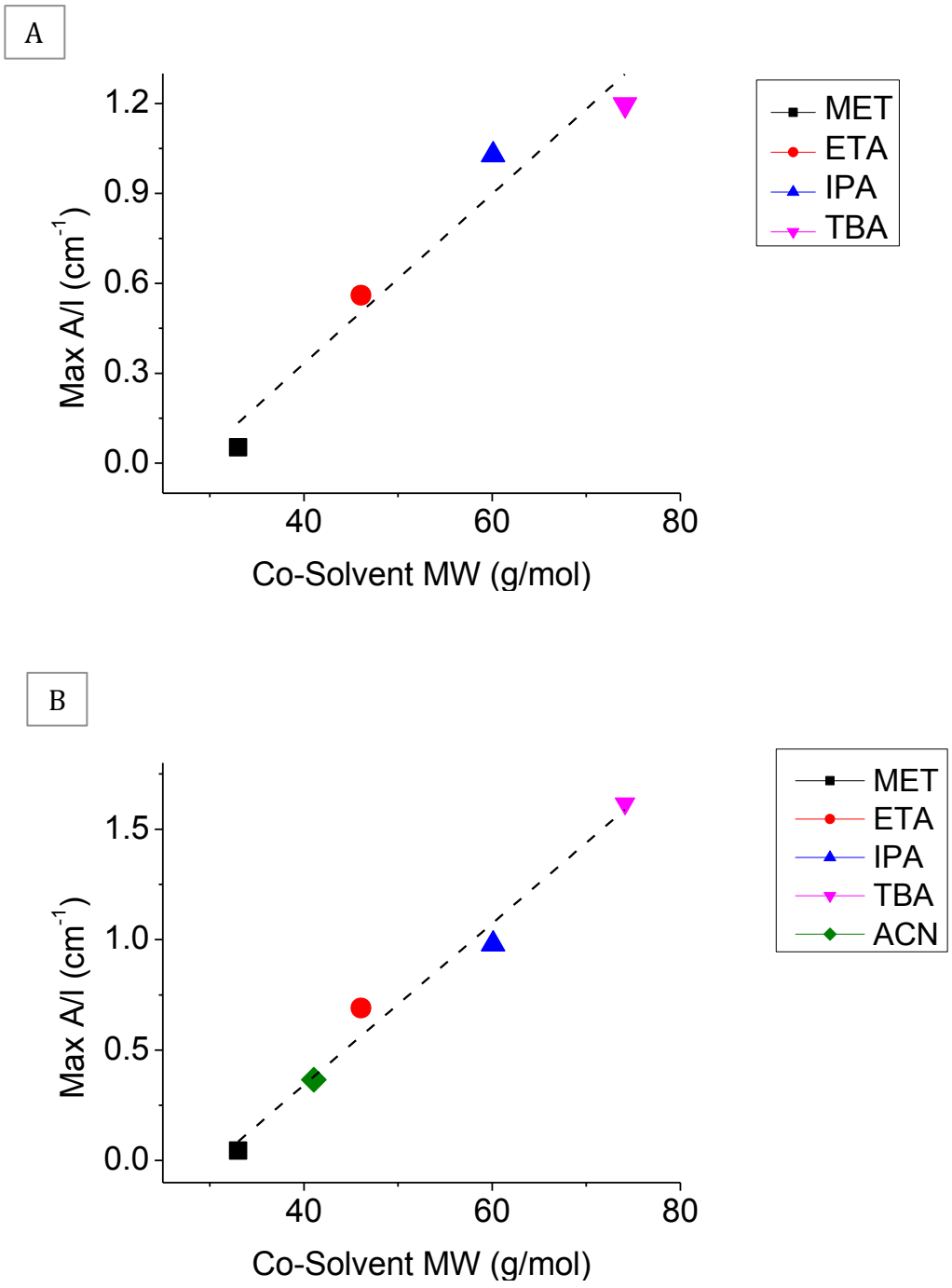

Figure 8. Maximum absorbance vs. co-solvent molecular weight for (A) graphene and (B) MoS_2.

4.2.2 Exfoliation Rate

We prepared our graphite and MoS2 samples in a different composition (in mass%) of Isopropanol-Water mixture for a range of sonication time. Data were measured in every one-hour period. As shown in Figure 9, 30 mass% of Isopropanol (surface tension ~27mN/m) has the highest exfoliation rate in both materials as compared to the other solvent composition and pure Isopropanol. This result is very important as it specifies that high exfoliation rate could only be obtained with solvents that qualify the solvent selection criterion as discussed above. Thus, suitable solvents not only can disperse the materials better but also exfoliate the materials faster.

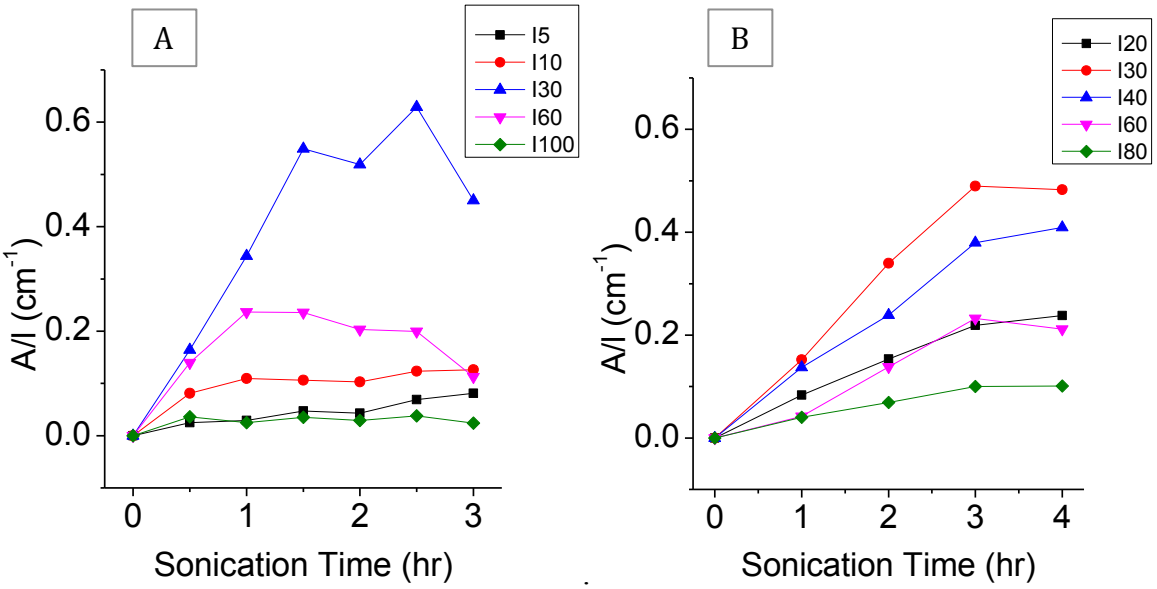

Figure 9. Absorbance of (A) graphene and (B) MoS_2 dispersed in different composition of Isopropanol-Water mixture as a function of sonication time.

4.3 Characterization of 2-D Flakes

The exfoliation state of the dispersed materials were analyzed with dispersion prepared by using 30 mass% of Isopropanol-Water mixtures. Thermal oxide wafer with 300nm SiO_2 on Si substrate was used for flake deposition. Then the average flake size, thickness and purity were characterized by SEM, AFM and TEM, respectively.

4.3.1 Scanning Electron Microscopy (SEM)

SEM images for flakes of graphene and MoS2 deposited on substrates are shown in Figure 10. From the images, very thin flakes, multilayers, and cluster of aggregated multilayers were observed. The SEM images show the deposited flakes with average lateral size range from 50nm to hundreds of nanometers for graphene and up to ~1μm size for MoS_2. Furthermore, smaller flakes were found to be restacked on the larger sheets.

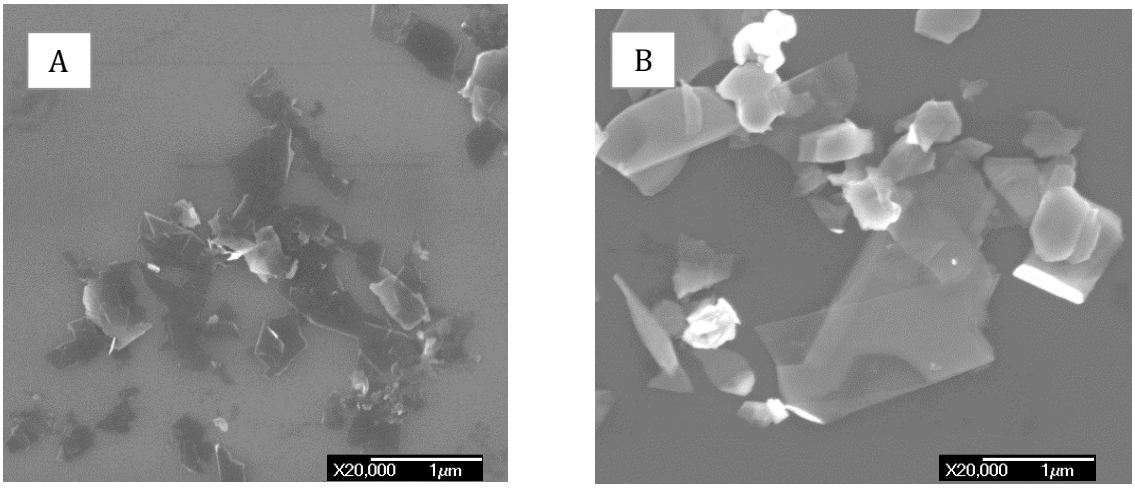

Figure 10. SEM images of (A) graphene and (B) MoS_2 flakes deposited on substrate.

4.3.2 Atomic Force Microscopy (AFM)

Sheets thickness was examined by AFM. Results shown that the thickness of graphene and MoS_2 flakes was around ~1nm for graphene and ~0.7nm for MoS_2. The thickness of pure monolayer graphene and MoS_2 sheet is around 0.34nm[1, 40] and 0.65nm [41], respectively. This suggests that the obtained graphene sheets consist of few layers while MoS_2 consists as single layer.

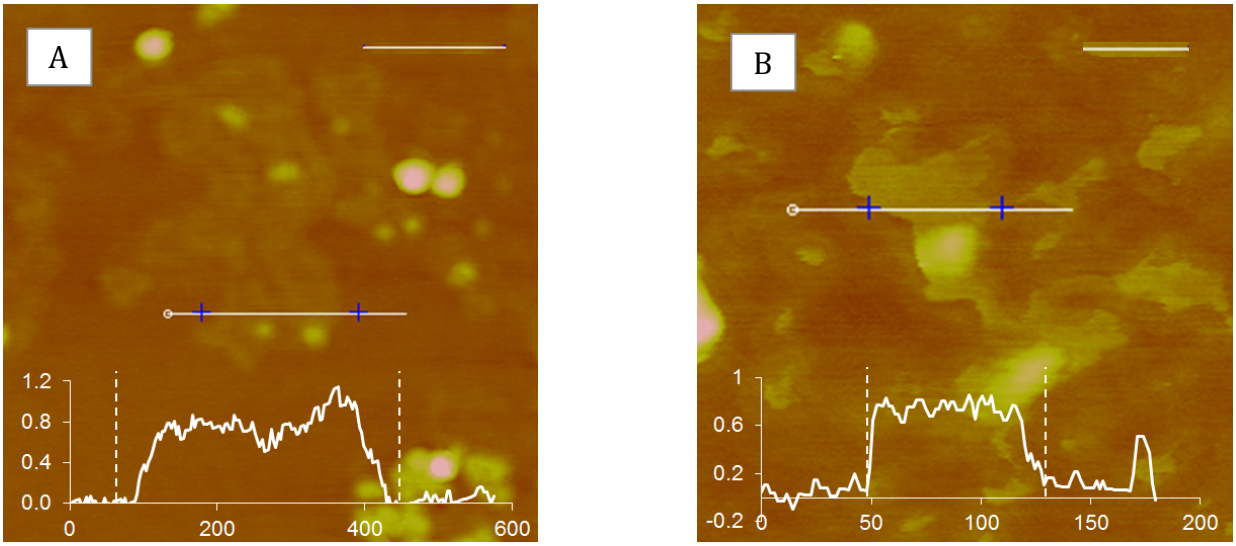

Figure 11. AFM images of (A) graphene and (B) MoS_2 nanosheets are deposited on substrate. Height profiles are corresponded to the white lines shown in the AFM images. The scale bars are 250nm 125 nm, respectively. Height profiles are shown in the scale of nanometers.

4.3.3 Transmission Electron Microscopy (TEM)

Under transmission electron microscopy analysis, large quantities of 2-D flakes consisting of thin nanosheets were observed. The associated Fast Fourier transforms indicated the presence of hexagonal symmetry for both materials, in which shows that materials were not damaged during the process. In the case of graphene, the diffraction pattern (inset of Figure 12A) clearly shows the {1100} and {2110} spots. The intensity ratio of the {1100} to the {2110} diffraction peaks reflects the existence of multilayer graphene [25] and is in a good consistency with the AFM results. High-resolution TEM images (Figure 13) show additional detailed structural information of the exfoliated nanosheets [20, 49]. These images clearly illustrate the hexagonal lattice for both materials. Again, it indicates that the exfoliated materials remained in their pristine structure.

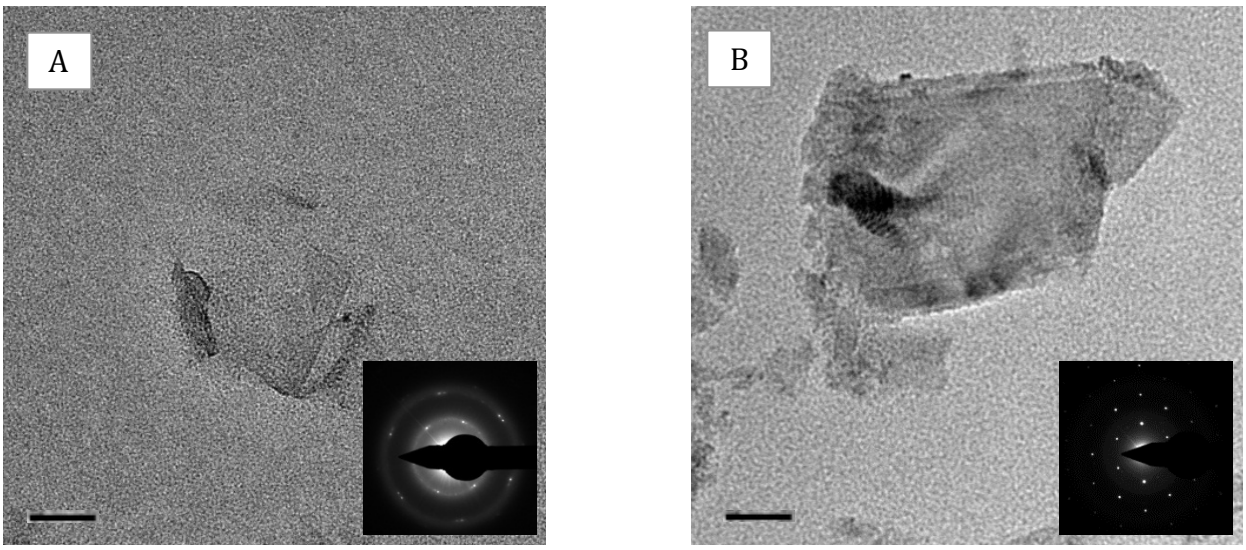

Figure 12. TEM images of flakes of (A) graphene and (B) MoS_2. The insets show the Fast Fourier transforms of the images. The scale bars are 20nm.

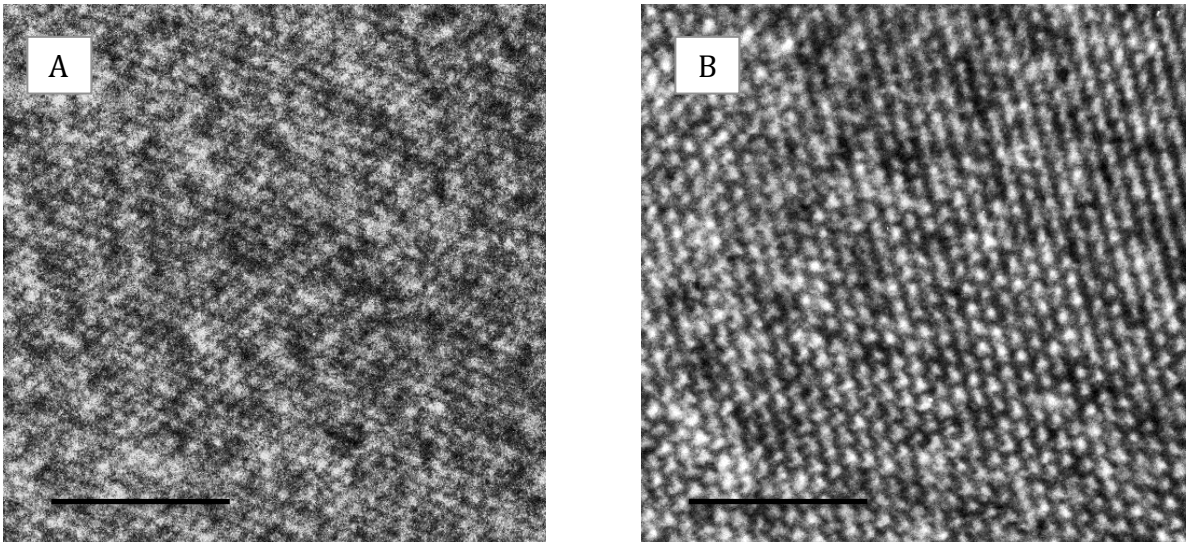

Figure 13. HRTEM images of exfoliated sheet of (A) graphene and (B) MoS_2. The scale bars are 3nm.

4.4 Characterizations of Deposited Films

When the ready-to-fabricate-graphene mixtures were added onto the water surface, co-solvents dissolved into water with forming a thin layer of insoluble butanol on the surface. At solubility equilibrium, the exfoliated materials would prefer to be suspended as a thin layer at the water-butanol interface due to its hydrophobic nature [45,46]. Then, as the butanol evaporated, the exfoliated materials would aggregate and form a uniform thin film on the water surface.

Dispersed graphene materials were fabricated into conductive films consist of nanosheets uniformly deposited on substrate (Figure 14). Transmittance measurements from 400nm to 1000nm were measured for graphene films fabricated with different thickness. The comparison of sheet resistance of graphene films with various thicknesses was analyzed by plotting sheet resistance as a function of percent transmittance (Figure 15).

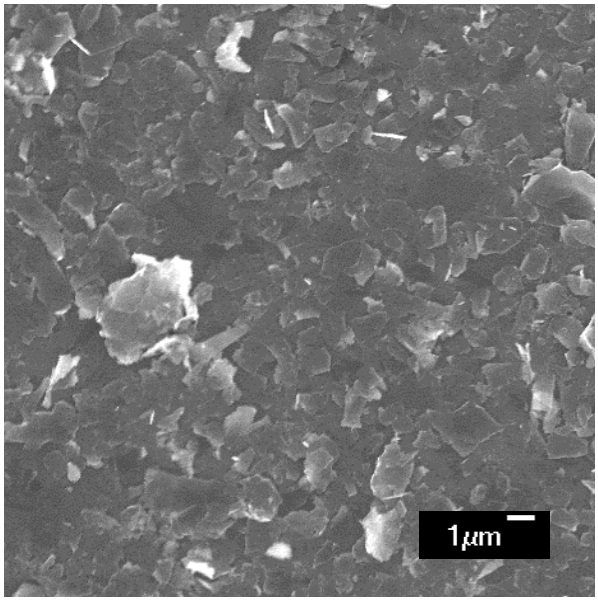

Figure 14. SEM image of the surface of graphene film deposited on substrate.

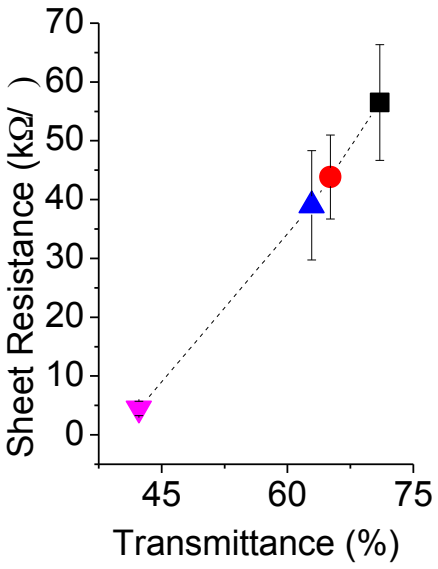

Figure 15. Sheet resistance as a function of percent transmittance for graphene films with various thicknesses.

Figure 15 reveals a strong correlation between the film transmittance and sheet resistance. Our graphene films with high transparency of 75% in transmittance have a sheet resistance value of ~55kΩ/□. Such high sheet resistance value might contribute to the poor interlayer junction contact within the films. Up to date, the best values of sheet resistance and transmittance reported in graphene based materials is reported with typical values of sheet resistance of 30Ω/□ at transmittance of 90% for graphene multilayers [42,43] and 8Ω/□ at transmittance of 84% for few-layer graphene intercalated with Ferric chloride [44]. Although our results showed that the principle works, further development with producing higher quality films with better performances is needed.

5

Summary, Conclusions and Future Work

In conclusion, this thesis has successfully demonstrated that mixture of common solvents with water can significantly improve the exfoliation of layered materials. A high yield of exfoliated materials was obtained from co-solvents with larger molecular size as it provides larger separation distance that significantly stabilizes the system. Thus, the recombinations between the layers are highly prevented. Efficiency of the solvent mixtures in the exfoliation process was examined under sonication time study. Overall performance for the solvent mixtures is ranked in the following from the best to the poorest: *tert*-Butanol-Water > Isopropanol-Water > Ethanol-Water > Acetonitrile-Water > Methanol-Water. Additionally, under detailed analysis, the resulting flakes are highly defect-free and oxide-free which consist only of a few layers.

Finally, a novel method with using the solvent stabilization theory has been introduced to prepare the exfoliated materials into thin films. A correlation between the transparency and the sheet resistance of graphene films made with different thicknesses was constructed. However, an unacceptably high sheet resistance value was obtained for the films. Therefore, the film fabrication process should be further investigated.

By using various low-boiling point mixtures with co-solvency approach, the fabricating process could become much more practical for industry. This process will not only offer obvious

advantages such as low cost, low toxicity, and easy removal; it will also give researches more freedom to engineer ideal solvent systems for each specific application.

Appendix

Surface Tension of Aqueous Mixtures

The composition dependence of the surface tension of binary mixtures of alcohol / acetonitrile with water is given in the following tables. The data are tabulated in the mass percent of the non-aqueous component ranging from 0% to 100%.

Table 1. Methanol + Water (at 25°C) [47]

mass % of Methanol	Surface Tension [mN/m]
0	72.01
10	56.18
20	47.21
30	41.09
40	36.51
50	32.86
60	29.83
70	27.48
80	25.54
90	23.93
100	22.51

Table 2. Ethanol + Water (at 25°C) [47]	
mass % of Ethanol	Surface Tension [mN/m]
0	72.01
10	47.53
20	37.97
30	32.98
40	30.16
50	27.96
60	26.23
70	25.01
80	23.82
90	22.72
100	21.82

Table 3. Isopropanol + Water (at 25°C) [47]	
mass % of Isopropanol	Surface Tension [mN/m]
0	72.01
10	40.42
20	30.57
30	26.82
40	25.27
50	24.26
60	23.51
70	22.68
80	22.14
90	21.69
100	21.22

Table 4. *tert*-Butanol + Water (at 25°C) [48]	
mass % of *tert*-Butanol	Surface Tension [mN/m]
0	71.97
10	33.93
20	26.03
30	23.81
40	23.20
50	22.93
60	22.70
70	22.17
80	21.17
90	20.93
100	20.10

Table 5. Acetonitrile + Water (at 20°C) [47]	
mass % of Acetonitrile	Surface Tension [mN/m]
0	72.8
10	48.5
20	40.2
30	34.1
40	31.6
50	30.6
60	30.0
70	29.6
80	29.1
90	28.7
100	28.4

7

References

1. K. S. Novoselov, A. K. Geim, S. V. Morozov, D. Jiang, Y. Zhang, S.V. Dubonos, I.V. Grigorieva, and A. A. Firsov, *Science* **306**, 666–669 (2004).
2. K. S. Novoselov, A. K. Geim, S. V. Morozov, D. Jiang, M. I. Katsnelson, I. V. Grigorieva, S. V. Dubonos, A. A. Firsov, *Nature* **438**, 197–200 (2005).
3. Y. Zhang, J. W. Tan, H. L. Stormer, P. Kim, *Nature* **438**, 201–204 (2005).
4. M. Y. Han, B. Oezyilmaz, Y. Zhang, P. Kim, *Phys. Rev. Lett.* **98**, 206805 (2007).
5. K. I. Bolotina, K. J. Sikesb, Z. Jianga,d, M. Klimac, G. Fudenberga, J. Honec, P. Kima, H. L. Stormer, *Solid State Commun.* **146**, 351–355 (2008).
6. C. Lee, X. Wei, J.W. Kysar, J. Hone, *Science* **321**, 385–388 (2008).
7. J. S. Bunch *et al., Science* **315**, 490–493 (2008).
8. J. K. Wassei and R. B. Kaner, *Materials Today* **13**, 52-59 (2010).
9. M.J. Allen *et al., Adv. Mater.* **21**, 1-5 (2009).
10. A. Kumar, C. Zhou, *ACS Nano* **4***,* 11 (2010)
11. D. S. Hecht, L. Hu, G. Irvin, *Adv. Mater.* **23**, 1482 (2011).
12. H. Park, J. Park, A. K. L. Lim, E. H. Anderson, A. P. Alivisatos, P. L. McEuen, *Nature* **407**, 57-60 (2000).
13. K.F. Mak, C. Lee, J. Hone, J. Shan and T. F. Heinz, *Phys. Rev. Lett.* **105,** 136805 (2010).
14. A. Kumar and P.K. Ahluwalia, *Eur. Phys. J. B* **85**, 186 (2012).

15. X. Li, W. Cai, J. An, S. Kim, J. Nah, D. Yang, R. Piner, A. Velamakanni, I. Jung, E. Tutuc, S. K. Banerjee, L. Colombo, R. S. Ruoff, *Science* **324**, 1312-1314 (2009).

16. Y. Zhan, Z. Liu, S. Najmaei, P. M. Ajayan, J. Lou, *Small* **8,** 966-971 **(**2012).

17. Y. Shi, C. Hamsen, X. Jia, K. K. Kim, A. Reina, M. Hofmann, A. L. Hsu, K. Zhang, H. Li, Z. Juang, M. S. Dresselhaus, L. Li, and J. Kong, *Nano Lett.***10**, 4134–4139 (2010).

18. D. Golbery, *Nature Nanotechnology* **6**, 200–201 (2011).

19. G. F. Walker, *Nature* **187**, 312-313 (1960).

20. J. N. Coleman, M. Lotya, A. O'Neill, S. D. Bergin, P. J. King, U. Khan, K. Young, A. Gaucher, S. De, R. J. Smith, I.V. Shvets, S. K. Arora, G. Stanton, H. Kim, K. Lee, G. T. Kim, G. S. Duesberg, T. Hallam, J. J. Boland, J. J. Wang, J. F. Donegan, J. C. Grunlan, G. Moriarty, A. Shmeliov, R. J. Nicholls, J. M. Perkins, E. M. Grieveson, K. Theuwissen, D. W. McComb, P. D. Nellist, V. Nicolosi, *Science* **331,** 568 (2011).

21. K. Zhou, N. Mao, H. Wang, Y. Peng, H. Zhang, *Angew. Chem. Intl. Ed.* **50,** 10839-10842 (2011).

22. X. Huang, Z. Yin, S. Wu, X. Qi, Q. He, Q. Zhang, Q. Yan, F. Boey, H. Zhang, *Small* **7,** 1876-1902 (2011).

23. M.N. McCain, J. Bo He, Q.J. Sanati, J.T. Wang, Marks, *Chem. Mater.* **20**, 5438 (2008).

24. M M Benameur, B Radisavljevic, J S Héron, S Sahoo, H Berger, A Kis, *Nanotechnology* **22,** 125706 (2011).

25. Y. Hernandez, V. Nicolosi, M. Lotya, F. M. Blighe, Z. Sun, S. De, I. T. McGovern, B. Holland, M. Byrne, Y. K. Gun'Ko, J. J. Boland, P. Niraj, G. Duesberg, S. Krishnamurthy, R. Goodhue, J. Hutchison, V. Scardaci, A. C. Ferrari, J. N. Coleman, *Nature Nanotechnology* **3**, 563 - 568 (2008).

26. G. Cunningham *et al., ACS Nano* ***6***, 3468–3480 (2012)

27. S. D. Bergin, V. Nicolosi, P. V. Streich, S. Giordani, Z. Sun, A. H. Windle, P. Ryan, N. P. P. Niraj, Z. T. Wang, L. Carpenter, W. J. Blau, J. J. Boland, J. P. Hamilton, J. N. Coleman*, Adv. Mater*. **20**, 1876 (2008).

28. A. Gordon, D. Yang, E. D. Crozier, D. T. Jiang, R. F. Frindt*, Phys. Rev. B* **65**, 125407 (2002).

29. Hansen, C. M. *Hansen Solubility Parameters - A User's Handbook*; CRC Press: Boca Raton, FL, **2007**.

30. F. D. Miles, *Cellulose Nitrate*; Oliver and Boyd: Edinburgh, Scotland, 1955; Chapter 5.

31. L. P. Cheng, H. Y. Shaw, J. *Polym. Sci. B Polym. Phys*. **38**, 747–754 (2000).

32. F. Tanaka, T. Koga, H. Kojima, N. Xue, & F. M. Winnik**,** *Macromolecules* **44**, 2978–2989 (2011).

33. J. M. G. Cowie, M. A. Mohsin, I. J. McEwen, *Polymer* **28,** 1569 (1987).

34. P. C. Deb, S. Palit, *Die Makromol. Chem.* **166,** 227-234 (1973).

35. D. Li, M. B. Müller, S. Gilje, R. B. Kaner, G. G. Wallace*, Nature Nanotechnology* **3**, 101 - 105 (2008).

36. E. A. Ponomarev *et al., Thin Solid Films* **280,** 86-89 (1996).

37. S. Wang *et al., Langmuir* **25**, 11078-11081 (2009).

38. K. Weiss & J.M. Philips, *Physical Review B (Solid State)* **14***,* 5392-5395 (1976).

39. C. Shih *et al., J. Am. Chem. Soc.***132**, 14638–14648 (2010).

40. X. Dong *et al., Phys. Chem. Chem. Phys.* **12**, 2164–2169 (2010).

41. B. Radisavljevic *et al., Nature Nanotechnology* **6**, 147–150 (2011)

42. S. Bae, *et al., Nature Nanotechnology* **5,** 574–578(2010).

43. Y. Wang, *et al., Adv. Mater.* **23***,* 1514 (2011).

44. I. Khrapach et al., *Adv. Mater.* **24***,* 2844–2849 (2012).

45. X. Zhang, S. Wan, J. Pu, L. Wang, X. Liu, *J. Mater. Chem.* **21**, 12251-12258 (2011).

46. O. Leenaerts, B. Partoens, F. M. Peeters, *Phys. Rev. B* **79,** 235440 (2009).

47. D. R. Lide, *CRC Handbook of Chemistry and Physics,* 84th Edition; CRC Press: Boca Raton, FL, **2003**.

48. J. Glinski, G. Chavepeyer, J. Platten, *The Journal of Chemical Physics, **102,** 2113-2117 (1995).*

49. J. H. Warner, M. H. Rümmeli, L. Ge, T. Gemming, B. Montanari, N. M. Harrison, B. Büchner, G. A. D. Briggs, *Nature Nanotechnology* **4**, 500 - 504 (2009).

50. K. K. Chawla, *Composite Materials: Science and Engineering,* 2nd Edition; Springer-Verlag New Yok, Inc. New York, NY, **1998**.

51. Y. Tanaka, Y. Matsuda, H. Fujiwara, H. Kubota, T. Makita, *International Journal of Thermophysics* **8**, 147-163 (1986).